Rare Metal Materials and Engineering
Volume 55, Issue 8, August 2026
Available online at www.rmme.ac.cn

Science Press

Cite this article as: Hu Chunyan, Dong Meijing, Liu Xinling, et al. Effect of Gas Film Holes Processing Technique and Adjacent Hole Spacing on Oxidation Behavior of DD6 Single-Crystal Superalloy[J]. Rare Metal Materials and Engineering, 2026, 55(08): 1907-1916. DOI: https://doi.org/10.12442/j.issn.1002-185X.20250472.

ARTICLE

Effect of Gas Film Holes Processing Technique and Adjacent Hole Spacing on Oxidation Behavior of DD6 Single-Crystal Superalloy

Hu Chunyan[1,2], Dong Meijing[3], Liu Xinling[1,2], Chen Xing[1,2], Liu Changkui[1,2]

[1] AECC Beijing Institute of Aeronautical Materials, Beijing 100095; [2] Beijing Key Laboratory of Aeronautical Materials Testing and Evaluation, Beijing 100095; [3] Institute of Metal Research, Chinese Academy of Sciences, Shenyang 110016

Abstract: This study employed a field emission scanning electron microscope, an energy dispersive spectroscope, and ABAQUS finite element analysis to investigate the oxidation behavior of DD6 single-crystal superalloy at a constant temperature of 1000 ℃, focusing on the effects of various processed drilling processes and adjacent hole spacting. The results show that the trend in oxidation mass gain of the DD6 single-crystal superalloy processed by different drilling techniques with different adjacent hole spacting is relatively consistent, following the order: 0.75 mm>0.95 mm>0.55 mm>0.39 mm. Compared with drilling process, adjacent hole spacting emerges as the primary factor affecting oxidation mass gain. The high-temperature oxidation behavior differs between the two drilling processes. The change in microstructure and elemental redistribution in the recast layer produced by electrical discharge machining may cause a variety of elements at different states to react at different rates simultaneously. In contrast, after femtosecond laser processing, there is almost no recast layer on the inner wall of the holes, and the oxide layer forms directly on the single-crystal alloy matrix. Finite element analysis reveals that oxide layer developed on hole surfaces is primarily governed by shedding stress. As adjacent hole spacing increases, the areas of stress cancellation diminish, while shedding stress escalates to a peak under the adjacent hole spacing of 0.75 mm, at which point oxide film shedding is the most pronounced, and then decreases.

Key words: gas film holes; single-crystal superalloy; EDM drilling; femtosecond laser drilling; oxidation behavior; shedding stress

1 Introduction

Turbine blades have complex structures and must withstand complex loads and high temperatures. To increase the turbine inlet temperature and the high-temperature resistance of turbine blades, there are currently three main methods. (1) Select materials with high-temperature resistance, gas-corrosion resistance, and certain strength and hardness. (2) Apply thermal barrier coatings on the blade surface to enhance the high-temperature resistance and corrosion resistance of the engine blades. (3) Use film cooling technique to cool the turbine blades[1]. However, the temperature of local areas of the film cooling holes can still reach 1100 ℃ under certain conditions. Moreover, due to their structural characteristics, it is difficult to apply thermal barrier coatings inside the holes, making them prone to severe oxidation and corrosion when exposed to high temperatures for long periods, and leading to premature failure of the blades in harsh service environments[2].

Currently, the film-cooling holes in turbine blades are mainly processed by electrical discharge machining (EDM), electro-hydraulic forming, and femtosecond laser[3]. Different processing methods cause various damage. For example, EDM is a thermal processing method, and the surface of the film-cooling holes has varying degrees of recast layers and microcracks[4]. Electro-hydraulic forming can cause edge corrosion damage to the holes, and the femtosecond laser process is not yet mature and sometimes leaves prismatic marks on the hole walls. Due to significant differences in the

Received date: September 16, 2025
Foundation item: National Science and Technology Major Project (J2019-Vl-0022-0138); Institute Fund of AECC Beijing Institute of Aeronautical Materials (KJSZ240769)
Corresponding author: Hu Chunyan, Ph. D., Senior Engineer, AECC Beijing Institute of Aeronautical Materials, Beijing 100095, P. R. China, Tel: 0086-10-62496238, E-mail: fachcy@163.com

microstructures between the film-cooling holes and the base material and the redistribution of elements around the holes during processing, the high-temperature oxidation behavior of the film-cooling holes processed by different methods is different from that on the surface of base material. The oxide layer produced around the film cooling holes is more brittle compared to that around the base material, and the strength of the γ' phase disappearance layer caused by element diffusion is also lower than that of the base material, making it an important area for crack initiation during loading[2]. However, most research on the influence of film-cooling holes on turbine blades have focused on the impact of hole distribution and geometric configuration on the cooling performance of turbine blades[5–9]. Therefore, studying the influence of different hole processing methods and adjacent hole spacings on the oxidation behavior of single-crystal superalloy is of great significance.

In this work, DD6 single-crystal superalloy was selected as the research object, and two different processing methods, including EDM drilling and femtosecond laser drilling, were used. The effects of different hole processing methods and adjacent hole spacings on the oxidation behavior of single-crystal superalloys were analyzed. This research not only provides a reference for the processing and design of film-cooling holes in engineering, but also has certain guiding significance for the failure analysis of film-cooling holes in single-crystal blades.

2 Experiment

The nominal chemical composition of the DD6 single-crystal superalloy used in the experiment was 4.3wt% Cr, 9.0wt% Co, 2.0wt% Mo, 48.0wt% W, 7.5wt% Ta, 2.0wt% Re, 0.5wt% Nb, 5.6wt% Al, 0.1wt% Hf, 0.006wt% C, and the balanced Ni. The DD6 single-crystal superalloy test bars were prepared in a high-temperature-gradient vacuum directional-solidification furnace by the helical crystal selection method and heat-treated according to the standard regime. The crystal orientation of the samples was [001]. All samples were examined for crystal orientation using X-ray Laue back-scattering method, with the deviation angle within 10°.

The appearance of the perforated oxidized plate is shown in Fig. 1. The size of the sample was 30 mm×10 mm×1.5 mm, and the number of holes on each sample was 43. EDM drilling and femtosecond laser drilling techniques were used to process the holes, and the angles of the holes were all 45° to simulate the distribution of holes in the leading edge of the real blade. The adjacent hole spacings were designed to be 0.39, 0.55, 0.75, and 0.95 mm, and the holes were all 0.40 mm in diameter.

A constant temperature oxidation test was conducted using static mass-gain method at the test temperature of 1050 ℃ for 600 h. The samples were removed, observed, and weighed every 25 h before returning to the furnace for continued oxidation. Each data point represents the average mass gain of three parallel samples.

The morphology and composition of oxidation products of different samples were observed and analyzed by a field emission scanning electron microscope (SEM, NOVA NANOSEM 450) and an energy-dispersive X-ray spectroscope (EDS). Focused ion beam (FIB) technique was used to cut slices of the samples in the hole wall's damage layer and the matrix, and the orientation and microstructure of the hole wall's damage layer and the matrix were observed by transmission electron microscope (TEM, JEOL-2010F). The effect of different adjacent hole spacings on the oxidation behavior of DD6 single-crystal superalloy was analyzed by ABAQUS finite element software.

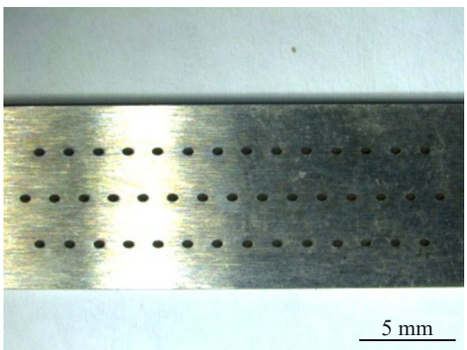

Fig.1 Appearance of the perforated oxidized plate

3 Results and Discussion

3.1 Oxidation kinetics curve

Fig. 2 shows the oxidation kinetics curves of DD6 single-crystal superalloy with different drilling processes and adjacent hole spacings during oxidation at 1000 ℃ for 600 h. It can be seen that the oxidation kinetics curves of samples prepared by EDM drilling and femtosecond laser drilling are different from those of the DD6 single-crystal superalloy itself[10–11] and do not completely follow the parabolic law. As oxidation progresses, the oxide film on the surface and the inner wall of the holes gradually sheds, reducing the ion diffusion distance and leading to a notable increase in oxidation rate over time.

The comparison shows that the oxidized mass gain of the samples prepared by EDM drilling is slightly higher than that prepared by the femtosecond laser drilling. However, for samples with different adjacent hole spacing processed by EDM drilling and femtosecond laser drilling, the oxidized mass gain follows the same trend: 0.75 mm>0.95 mm> 0.55 mm>0.39 mm. Among them, the sample with adjacent hole spacing of 0.75 mm grows faster than the rest, indicating that the effect of adjacent hole spacing is more significant than that of drilling process.

3.2 Oxidation product

Fig. 3 and Fig. 4 show the surface morphologies of oxide film of DD6 single-crystal superalloys with different drilling processes and distances between adjacent holes, respectively. Under the same adjacent hole spacing, the oxidation degree on the surface of sample prepared by EDM drilling is more serious than that prepared by femtosecond laser drilling. It is

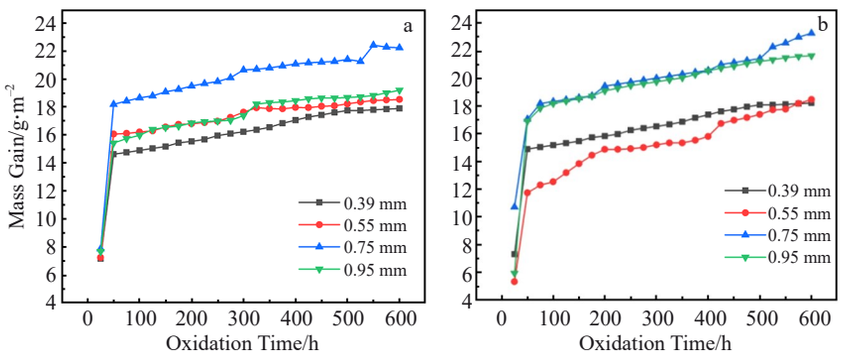

Fig.2 Oxidation kinetics curves of DD6 single-crystal superalloy with different drilling processes during oxidation at 1000 ℃ for 600 h: (a) EDM drilling; (b) femtosecond laser drilling

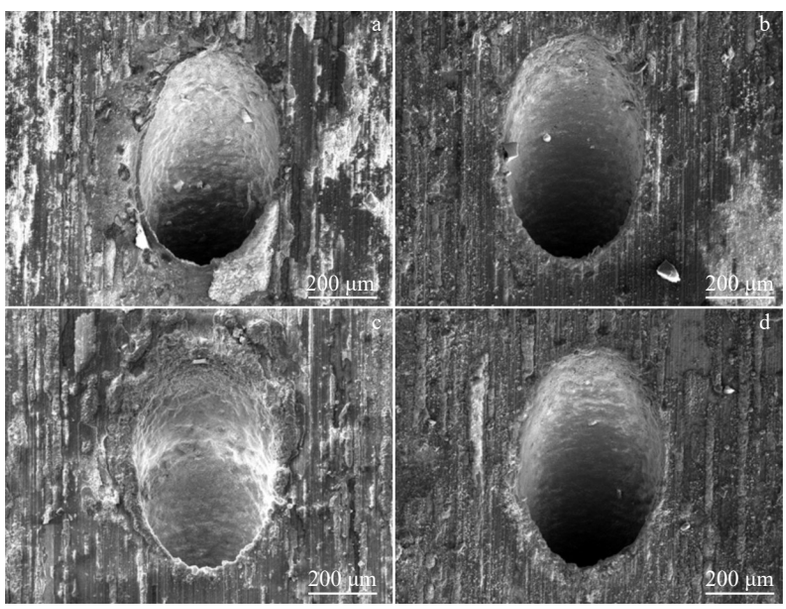

Fig.3 Surface oxidation morphologies of DD6 single-crystal superalloy prepared by EDM drilling with different adjacent hole spacings: (a) 0.39 mm, (b) 0.55 mm, (c) 0.75 mm, and (d) 0.95 mm

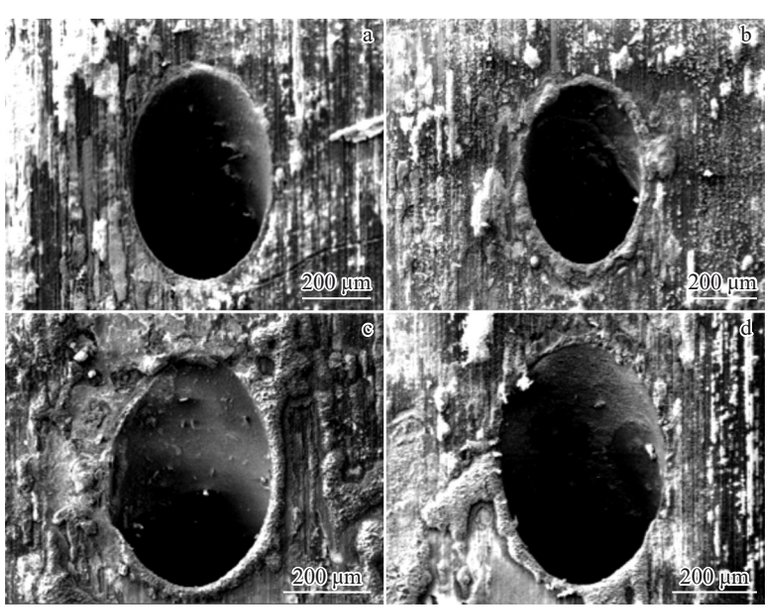

Fig.4 Surface oxidation morphologies of DD6 single-crystal superalloy prepared by femtosecond laser drilling with different adjacent hole spacings: (a) 0.39 mm, (b) 0.55 mm, (c) 0.75 mm, and (d) 0.95 mm

found that samples with adjacent hole spacing of 0.75 and 0.95 mm exhibit more pronounced oxidation, with thick oxidation products around the holes and significant shedding of the oxide film from the sample surfaces.

The surface oxidation morphology of DD6 single-crystal superalloy prepared by EDM drilling with a hole angle of 45° and the adjacent hole spacing of 0.75 mm is shown in Fig.5a. Combined with the EDS analysis, the protruding oxides on the surface are spinel oxide layer ($NiCr_2O_4$) and a small amount of NiO (Fig. 5b). At high magnification, the oxide formed at the hole edge exhibits a spinel-like morphology and is primarily composed of NiO (Fig. 5c). After the oxide film falls off, due to the lack of hindrance to the element O, a large number of NiO and $NiCr_2O_4$ are formed, the density of NiO increases gradually, and the grain size increases (Fig.5d)[12].

Fig. 6 and Fig. 7 show the cross-sectional oxidation morphologies around the holes of DD6 single-crystal superalloy with different adjacent hole spacings prepared by EDM drilling and femtosecond laser drilling, respectively. It can be seen that the oxide film around the holes of sample prepared by EDM drilling mainly has a double-layer structure, with the outermost (Ni, Co)O layer severely peeled off. Although the spinel oxide layer and Al_2O_3 layer remain continuous and dense, the cubic degree of the γ' phase is reduced. The oxide film around the holes of sample prepared by femtosecond laser drilling is relatively continuous and dense, and the γ' phase still shows the original cubic structure. The order of oxide film thicknesses around the holes of

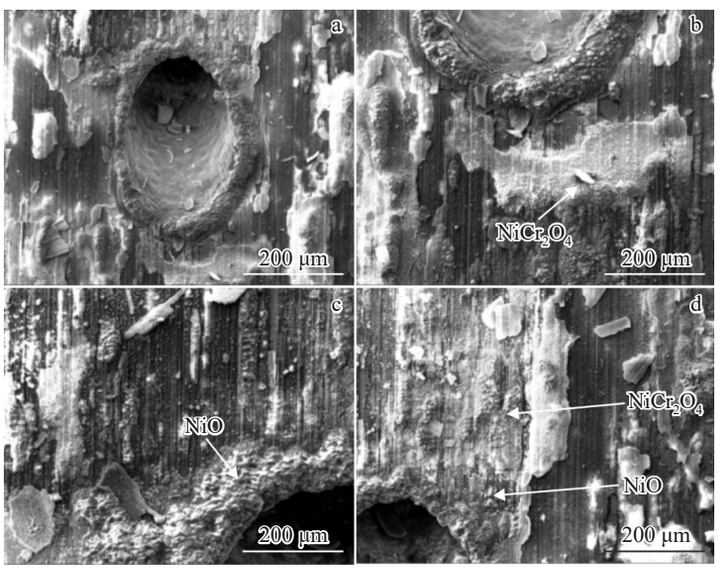

Fig.5 Oxidation morphologies of surface with adjacent hole spacing of 0.75 mm prepared by EDM drilling: (a) low-magnification morphology, (b) spinel oxide layer, (c) oxide at the edge of the hole, and (d) NiO and $NiCr_2O_4$

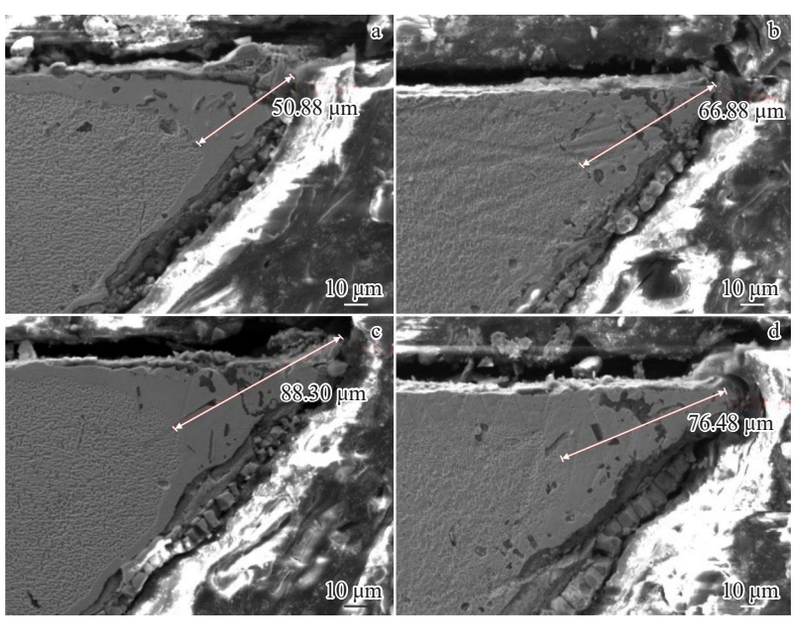

Fig.6 Cross-sectional oxidation microstructures around the hole of DD6 single-crystal superalloy with different adjacent hole spacings prepared by EDM drilling: (a) 0.39 mm, (b) 0.55 mm, (c) 0.75 mm, and (d) 0.95 mm

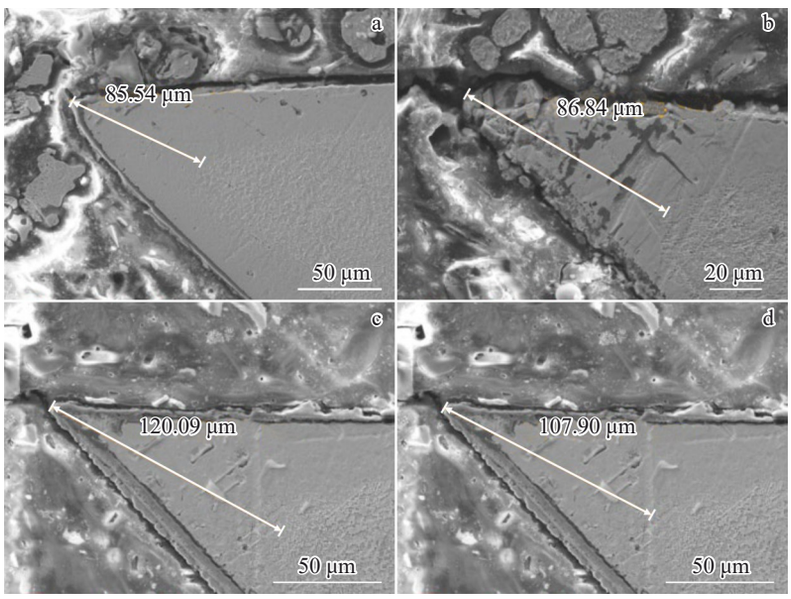

Fig.7 Cross-sectional oxidation microstructures around the hole of DD6 single-crystal superalloy with different adjacent hole spacings prepared by femtosecond laser drilling: (a) 0.39 mm, (b) 0.55 mm, (c) 0.75 mm, and (d) 0.95 mm

samples prepared by the two drilling processes is 0.75 mm>0.95 mm> 0.55 mm>0.39 mm, which is consistent with that of the previous oxidation mass-gain rule.

3.3 Influence of different drilling processes on oxidation behavior

The microscopic morphologies of different damage layers of DD6 single-crystal superalloy prepared by EDM drilling and femtosecond laser drilling are shown in Fig. 8. As EDM drilling is a thermal processing method, the high temperature induced by spark discharge, together with subsequent rapid quenching by the dielectric fluid, results in the formation of a recast layer with a specific thickness on the inner wall of the hole[13], as shown in Fig. 8a. In contrast, the femtosecond laser drilling has a different effect mechanism, in which the high energy density of the laser instantly melts and vaporizes the material. The alloy interacts briefly with oxygen, resulting in no significant recast layer on the inner wall of the holes. The γ' phase at the hole boundary retains better cubicity, leading to less damage than to EDM drilling (Fig.8b).

The chemical composition of recast layer, damage layers, and matrix is shown in Table 1. The Al content in the recast layer is lower than that in the matrix. Meanwhile, the damage layer shows a significant increase in O content relative to the matrix, along with slight increases in Al and Ta contents. This is due to the interaction between the laser and material. The material absorbs energy, undergoes vaporization or melting, and splashes away from the matrix. Some molten material cannot be fully discharged and condenses on the inner wall of hole, forming oxides.

Fig. 9 shows TEM analysis results of the damage layer of

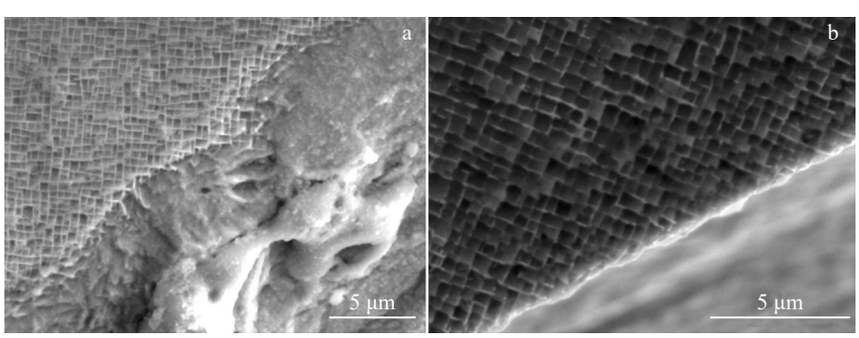

Fig.8 Microstructures of damage layer of samples prepared by different drilling processes: (a) EDM drilling; (b) femtosecond laser drilling

Table 1 Chemical composition of recast layer, damage layer, and matrix (wt%)

Region	O	Al	Ta	Cr	Ni	Co	W	Nb	Re	Mo
Recast layer (EDM drilling)	2.29	1.82	6.25	4.58	62.17	9.91	9.01	0.54	1.64	1.79
Damage layer (femtosecond laser drilling)	23.99	7.73	8.81	3.80	33.86	6.34	10.51	0.87	1.70	2.39
Matrix	1.85	4.67	6.21	5.07	58.27	9.67	9.17	1.98	2.89	2.20

sample prepared by EDM drilling. The recast layer is a γ'-free region, while the matrix exhibits a γ/γ' co-lattice arrangement. EDS analysis indicates that Al, Ni, and Ta are the main elements of the γ' phase, while other elements are predominant in the γ phase. The selected area electron diffraction (SAED) patterns reveal that the orientation of the recast layer is consistent with that of the matrix.

Fig.10 shows the TEM analysis results of the damage layer

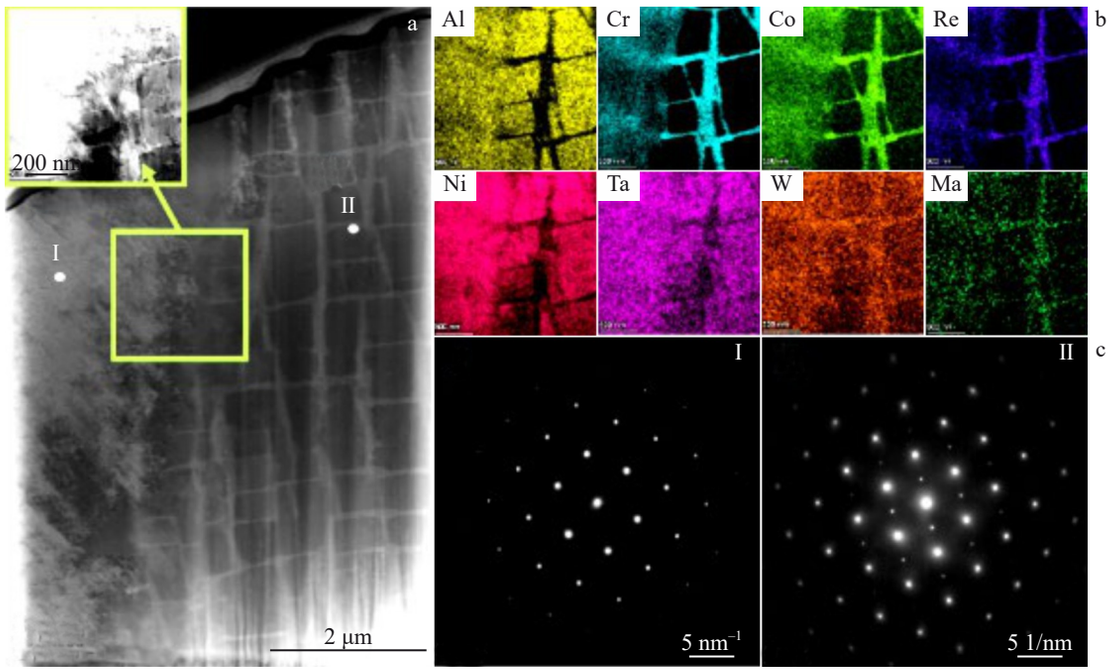

Fig.9 TEM image of the recast layer of sample prepared by EDM drilling (a), EDS element mappings of yellow square marked in Fig.9a (b), and SAED patterns of points I and II marked in Fig.9a (c)

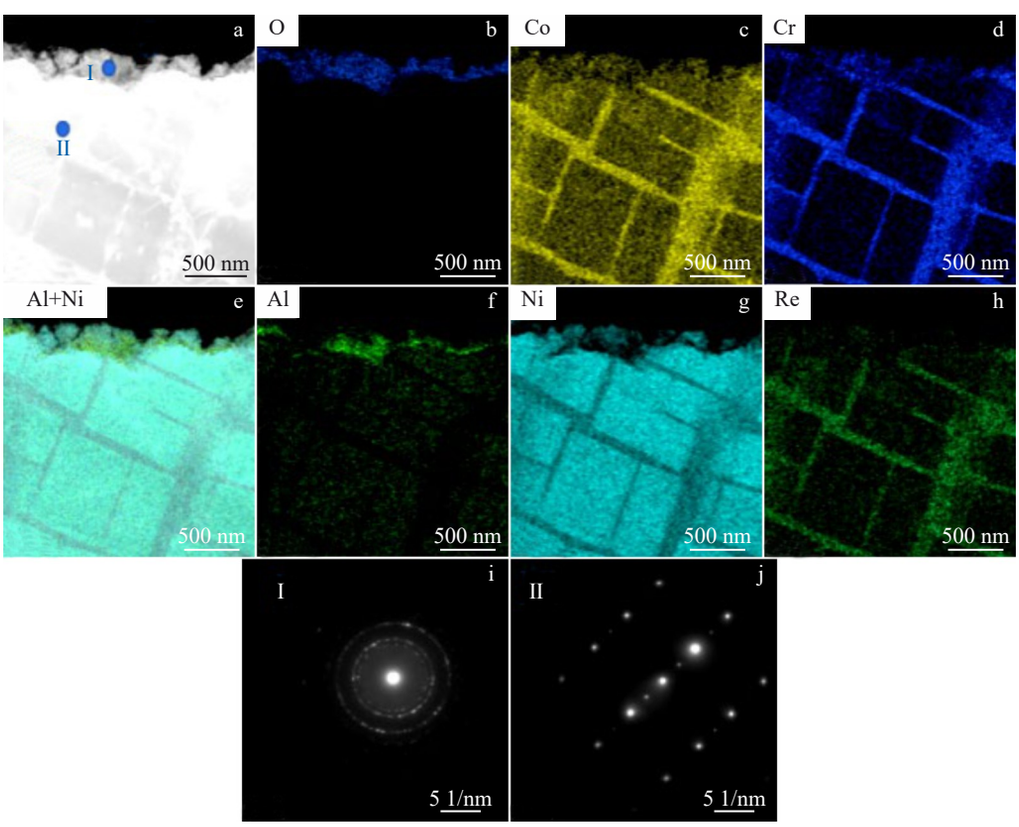

Fig.10 TEM image (a) and corresponding EDS element mappings (b–h) of the damage layer of sample prepared by femtosecond laser drilling: (b) O, (c) Co, (d) Cr, (e) Al+Ni, (f) Al, (g) Ni, and (h) Re; SAED patterns of points I (i) and II (j) marked in Fig.10a

of sample prepared by femtosecond laser drilling. There is almost no recast layer after femtosecond laser drilling, whereas there is a very thin layer of oxide at the outermost layer of the hole edge. This oxide layer primarily contains elements O and Al, along with Ni, Co, and Cr, which is consistent with the previous EDS analysis. The oxide exhibits a polycrystalline electron diffraction pattern.

3.4 Microstructure of oxide layer on the inner wall of holes

Fig. 11 shows the cross-section microstructures and corresponding EDS mappings of oxide layer of the sample prepared by the two drilling methods with adjacent hole spacing of 0.39 mm. The oxide film on the inner wall of the holes after EDM drilling is uneven, with a thicker oxide layer compared to that after femtosecond laser drilling, and the oxide layer Al_2O_3 is discontinuous near the innermost layer of the matrix.

The change in microstructure and elemental redistribution in the recast layer prepared by EDM drilling may cause a variety of elements in different states to react at different rates simultaneously. Due to the depletion of Al in the recast layer, crevices on the hole surface are prone to the formation of striated Al_2O_3, which lacks a continuous and dense microstructure (Fig. 11a), thereby enabling metal elements to diffuse through this layer more rapidly[14]. In contrast, after femtosecond laser drilling, there is almost no recast layer on the inner wall of the holes, and the oxide layer forms directly on the matrix. A three-layer oxide structure gradually develops, with the oxide layer on the inner wall of the holes being thinner and more uniform. The innermost Al_2O_3 layer is also continuous and dense (Fig. 11b), primarily due to the difference between the two drilling methods.

Fig. 12 shows the cross-section microstructures and corresponding EDS mappings of oxide layer of the sample prepared by the two drilling methods with adjacent hole spacing of 0.75 mm. Compared with the sample having a dadjacent hole spacing of 0.39 mm, the grain size of the outermost oxide NiO of sample with a adjacent hole spacing of 0.75 mm is obviously increased, accompanied by localized spalling. The oxide layer in areas without spalling is noticeably thicker, and the three-layer structure exhibits a continuous band-like distribution, which is mainly due to the differences caused by the adjacent hole spacing.

4 Finite Element Analysis of Hole Distribution on Oxidation Behavior

4.1 Meshing and material parameters

Based on the dimensions of the oxidized sample, a three-dimensional geometric model for finite element analysis was established and meshed. To obtain more accurate stress around the hole, the mesh around the hole edge was refined. The linearly reduced integration elements C3D8R were used. Fig.13 shows the meshed model.

According to Ref. [15], the stiffness matrix of Ni-based single-crystal superalloy is given by Eq. (1).

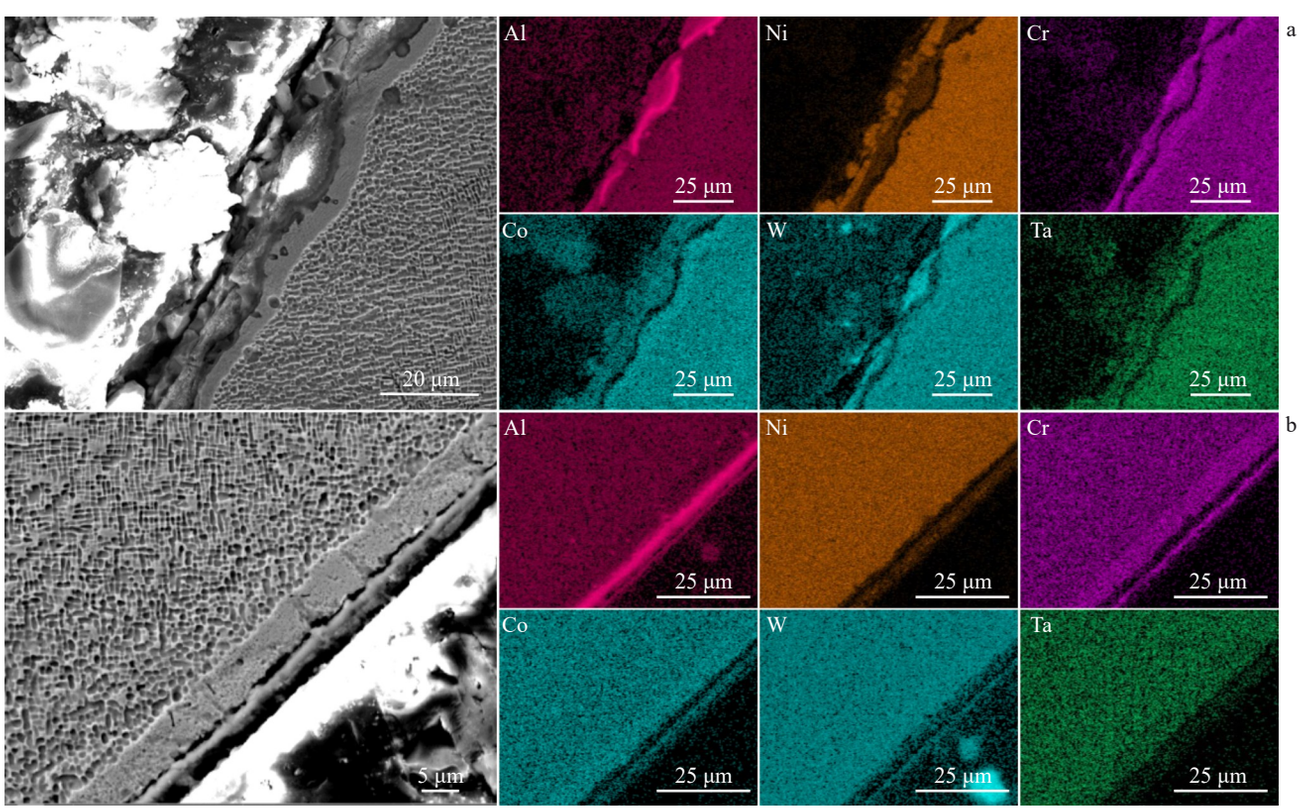

Fig.11 Cross-section microstructures and corresponding EDS mappings of oxide layer of the sample with adjacent hole spacing of 0.39 mm: (a) EDM drilling; (b) femtosecond laser drilling

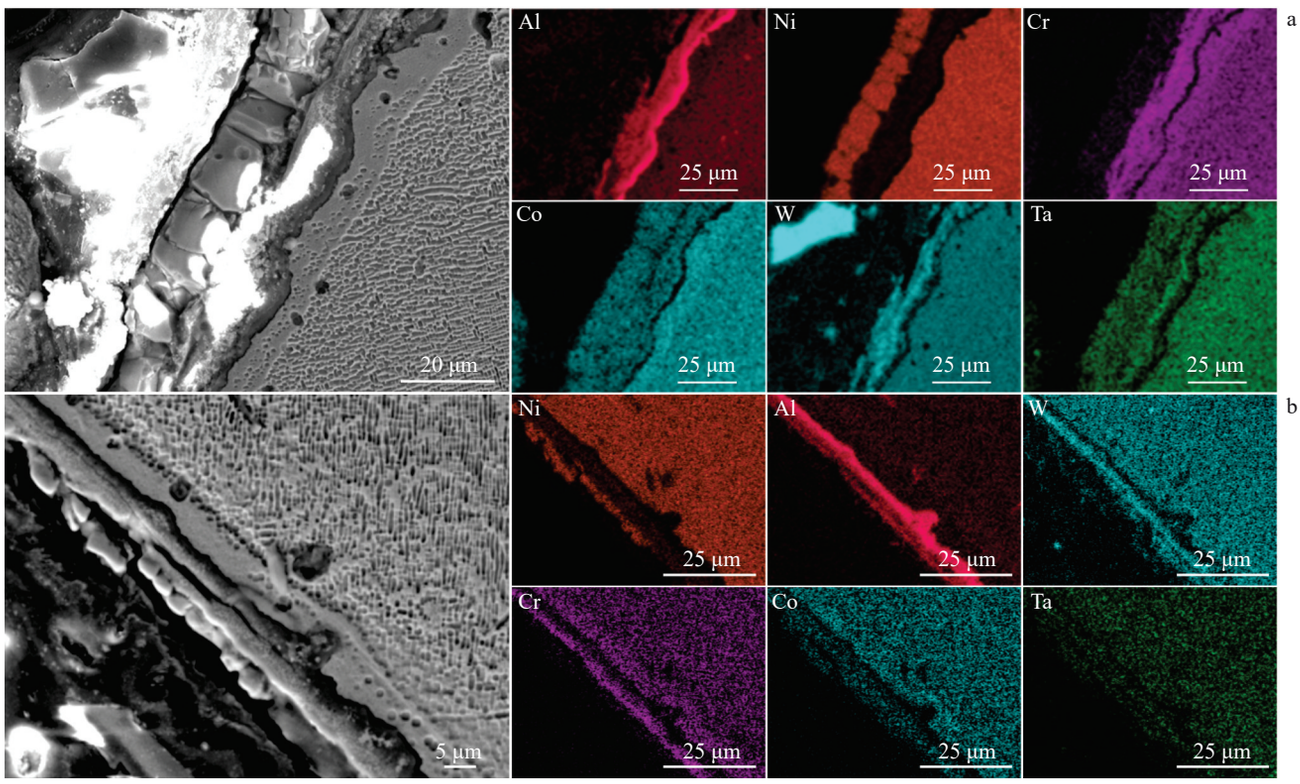

Fig.12 Cross-section microstructures and corresponding EDS mappings of oxide layer of sample with adjacent hole spacing of 0.75 mm: (a) EDM drilling; (b) femtosecond laser drilling

$$[C]=\begin{bmatrix} \frac{E(\mu-1)}{(2\mu-1)(\mu+1)} & \frac{-E\mu}{(2\mu-1)(\mu+1)} & \frac{-E\mu}{(2\mu-1)(\mu+1)} & & & \\ \frac{-E\mu}{(2\mu-1)(\mu+1)} & \frac{E(\mu-1)}{(2\mu-1)(\mu+1)} & \frac{-E\mu}{(2\mu-1)(\mu+1)} & & & \\ \frac{-E\mu}{(2\mu-1)(\mu+1)} & \frac{-E\mu}{(2\mu-1)(\mu+1)} & \frac{E(\mu-1)}{(2\mu-1)(\mu+1)} & & & \\ & & & G & & \\ & & & & G & \\ & & & & & G \end{bmatrix} \tag{1}$$

where $[C]$ is stiffness matrix; E is tensile and compressive elastic modulus in the crystal axis direction; G is shear modulus in the crystal axis direction; μ is Poisson's ratio in the crystal axis direction.

Some material parameters can be found in Ref. [16]. DD6 Ni-based single-crystal superalloy is orthotropic. At 1050 ℃, $E_{[001]}$ is 69.5 GPa, and Poisson's ratio μ is 0.399. The empirical formulas are shown in Eq. (2–3), as follows:

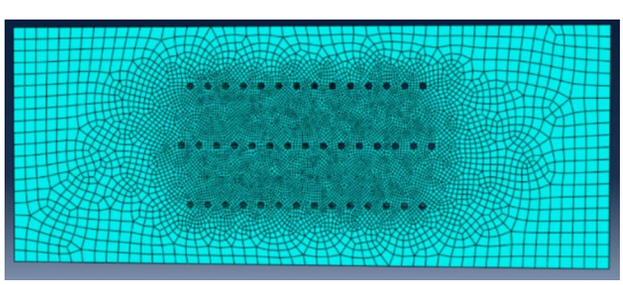

Fig.13 Schematic diagram of finite element mesh

$$\frac{1}{G}=\frac{4}{E_{[110]}}-\frac{2-2\mu}{E_{[100]}} \tag{2}$$

$$\frac{1}{G}=\frac{3}{E_{[111]}}-\frac{1-2\mu}{E_{[100]}} \tag{3}$$

where $E_{[110]}$ and $E_{[111]}$ are 130 and 189 GPa, respectively; shear modulus G is approximately 77 GPa. Substituting these material constants into Eq. (1), the stiffness matrix of DD6 superalloy is obtained.

4.2 Influence of adjacent hole spacing on oxide film shedding

Oxide layer growth will produce stress at the interface between the alloy matrix and the oxide layer, which is known as growth stress[17]. The growth stress at the gas film hole affects the stress state around the hole and of adjacent holes, which is a phenomenon referred to as the stress coupling superposition effect[18]. During the growth process, the oxide film will fall off due to several factors such as a mismatch of thermal expansion coefficient and thermal stress. After the

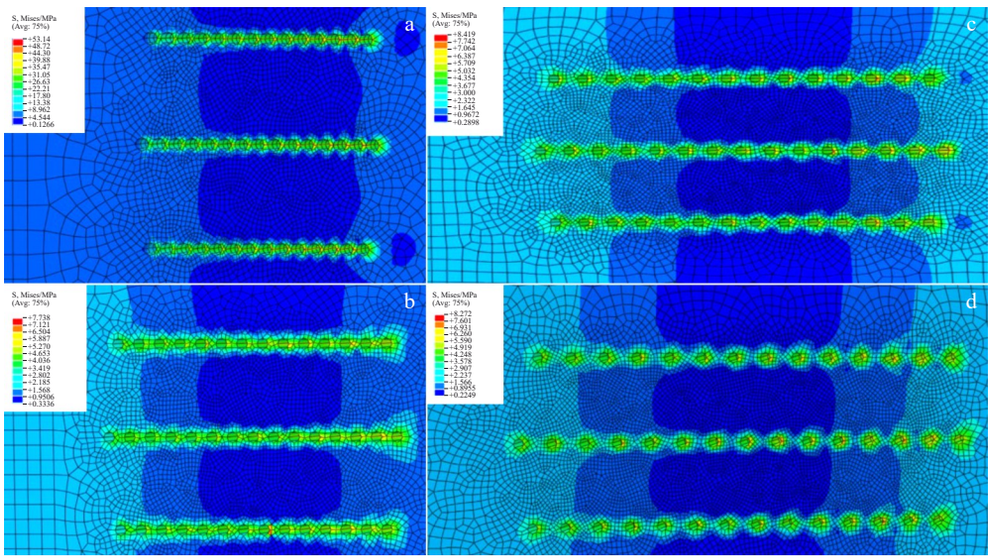

Fig.14 Growth stress distribution of samples with different adjacent hole spacings: (a) 0.39 mm, (b) 0.55 mm, (c) 0.75 mm, and (d) 0.95 mm

oxide film falls off, it lacks the blocking ability to element O, and the oxidation degree will be further aggravated.

Fig. 14 shows the stress distribution of samples with different adjacent hole spacing, simulated using ABAQUS. It can be observed that the coupling superposition effect in high-stress regions gradually weakens as adjacent hole spacing increases. A stress offset region exists between the holes, with the largest offset range at 0.39 mm, where the effect of shedding stress on the surface of hole is minimal. As the adjacent hole spacing increases, the stress offset region gradually decreases, the shedding stress increases, and there is a critical value of stress offset, with 0.75 mm being the closest to it. Therefore, at the adjacent hole spacing of 0.75 mm, oxide film shedding is the most pronounced, resulting in the most severe oxidation aggravation.

5 Conclusions

1) The oxidation mass gain of DD6 single-crystal superalloy shows consistent variation trend under different drilling processes and adjacent hole spacing, following the order of 0.75 mm>0.95 mm>0.55 mm>0.39 mm. The effect of adjacent hole spacing on oxidation mass gain is more significant compared to that of the drilling process.

2) The two drilling processes exhibit distinct high-temperature oxidation behaviors. The change in microstructure and elemental redistribution in the recast layer prepared by EDM drilling may cause a variety of elements in different states to react at different rates simultaneously. In contrast, after femtosecond laser drilling, there is almost no recast layer on the inner wall of the holes, and the oxide layer forms directly on the single-crystal superalloy matrix.

3) The growth of the oxide layer on the hole surface is mainly affected by the shedding stress. As the adjacent hole spacing increases, the stress offset region gradually decreases, while the shedding stress increases, peaking at 0.75 mm, where oxide film shedding is the most severe.

References

1 Liu X L, Wu X C, Li Z. *Failure Analysis and Prevention*[J], 2023, 18(1): 21

2 Yan Y Z, Yang Z, Zhao Y S *et al. Journal of Aeronautical Materials*[J], 2022, 42(2): 29

3 Yang Yongli. *Research on High Speed Electric Spark Processing for Gas Film Holes of High Pressure Turbine Blade*[D]. Dalian: Dalian University of Technology, 2008 (in Chinese)

4 Li Z W, Wen Z X, Wang P *et al. Failure Analysis and Prevention*[J], 2023, 18(1): 1

5 Li G C, Zhu H R, Bai J T *et al. Journal of Propulsion Technology*[J], 2008, 29(2): 153

6 Li Lei, Hou Naixian, Ao Liangbo *et al. Rare Metal Materials and Engineering*[J], 2013, 42(3): 519 (in Chinese)

7 Yu Q M, Wang Y L, Wen Z X *et al. Materials Science and Engineering A*[J], 2009, 520: 1

8 Hu C Y, Liu X L, Liu C K *et al. Failure Analysis and Prevention*[J], 2023, 18(1): 8

9 Sun Xinghua. *Study of Endurance Life Predict for Turbine Blade with Film Cooling Holes*[D]. Dalian: Dalian University of Technology, 2008 (in Chinese)

10 Shi Z X, Li J R, Liu S Z. *Transactions of Nonferrous Metals Society of China*[J], 2012, 22(3): 528

11 Zhang Z H, Meng J. *Journal of Chinese Society for Corrosion and Protection*[J], 2010, 30(4): 337

12 Liu Chengbao, Li Hui, Lou Langhong. *Rare Metal Materials and Engineering*[J], 2010, 39(8): 1407 (in Chinese)

13 Chen C J, Guo W Y, Wang M C *et al. Journal of Gas Turbine Experiment and Research*[J], 2004, 17(3): 44

14 Yang Y Z, Yang Z, Zhao Y S *et al. Journal of Aeronautical Materials*[J], 2022, 42(2): 29

15 Aerospace Engine Design Materials Data Handbook Editorial

Committee. *Aerospace Engine Design Materials Data Handbook* [M]. Beijing: Aviation Industry Press, 2010 (in Chinese)

16 Pei Haiqing. *The High-Temperature Oxidation and Thermal Fatigue Behaviors of Nickel-Based Single Crystal Superalloy* [D]. Xi ' an: Northwestern Polytechnical University, 2019 (in Chinese)

17 Akhtar A, Hook M S, Reed R C. *Metallurgical and Materials Transactions A*[J], 2005, 36: 3001

18 Atherya C N, Deepak K, Dong-Ik K *et al*. *Journal of Alloys and Compounds*[J], 2019, 778: 224

气膜孔加工工艺与孔间距对DD6单晶高温合金氧化行为的影响

胡春燕[1,2]，董美静[3]，刘新灵[1,2]，陈　星[1,2]，刘昌奎[1,2]

(1. 中国航发北京航空材料研究院，北京 100095)

(2. 航空材料检测与评价北京市重点实验室，北京 100095)

(3. 中国科学院金属研究所，辽宁 沈阳 110016)

摘　要：采用场发射扫描电子显微镜、能谱仪和ABAQUS有限元分析，研究了不同气膜孔加工工艺和孔间距对DD6单晶高温合金在1000 ℃恒温下氧化行为的影响。结果表明：采用不同打孔工艺和孔间距下，DD6单晶高温合金的氧化增重趋势一致，孔间距排序为0.75 mm>0.95 mm>0.55 mm>0.39 mm，孔间距对单晶高温合金氧化行为的影响比打孔工艺的影响更为显著。两种打孔工艺的高温氧化行为有所不同，电火花打孔产生的再铸层由于微观结构的变化和元素重新分布，导致不同的元素以不同速率发生反应。而飞秒激光打孔后，孔内壁几乎没有再铸层，氧化层直接在单晶高温合金基体上形成。有限元模拟结果表明，孔表面氧化层生长主要受氧化膜脱落应力的影响；随着孔间基体尺寸的增大，应力抵消区域逐渐减小，而氧化膜的脱落应力不断增大，并在孔间距为0.75 mm时达到峰值，此时的氧化膜脱落最为严重，之后又呈逐渐下降的趋势。

关键词：气膜孔；单晶高温合金；电火花打孔；飞秒激光打孔；氧化行为；脱落应力

作者简介：胡春燕，女，1983年生，博士，高级工程师，中国航发北京航空材料研究院，北京 100095，电话：010-62496238，E-mail：fachcy@163.com